Electronic Supplementary Information

Dual-Functional Iodine Photoelectrode Enabling High Performance Photo-assistant Rechargeable Lithium Iodine Batteries

Jingfa Li[a*], Hongmin Liu[a], Kaiwen Sun[b], Ronghao Wang[a], Chengfei Qian[a], Feng Yu[a], Lei Zhang[a], Weizhai Bao[a*]

[a] School of Chemistry and Materials Science
Nanjing University of Information Science & Technology
Nanjing, 210044, China.
E-mail: aplijf@nuist.edu.cn; weizhai.bao@nuist.edu.cn
[b] Australian Centre for Advanced Photovoltaics
School of Photovoltaic and Renewable Energy Engineering
University of New South Wales
Sydney, Australia 2052.

The working principle of the proposed photo-assisted rechargeable Li-I_2 battery can be summarized as follows:

Photoassisted charge-Cathode:

$Dye + hv \rightarrow Dye^*$ step 1

$Dye^* + TiO_2 \rightarrow TiO_2\text{-}Dye^+ + TiO_2\text{-}Dye^-$ step 2

$3I^- + 2Dye^+ \rightarrow I_3^- + 2Dye$ step 3

Anode:

$Li^+ + e^- \rightarrow Li$ step 4

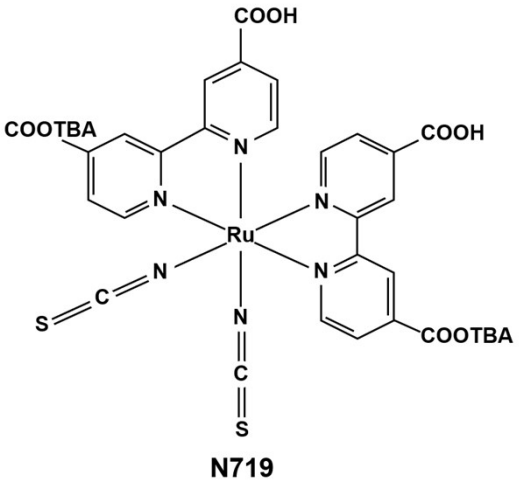

Figure S1. Structure of dye N719.

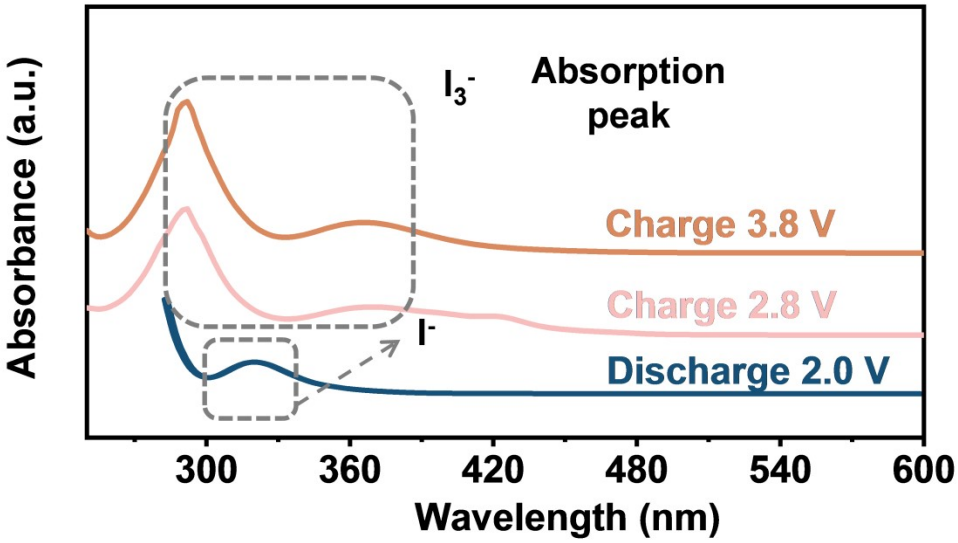

Figure S2. Ultraviolet-visible spectrum of the electrolyte used after cycling under illuminated conditions.

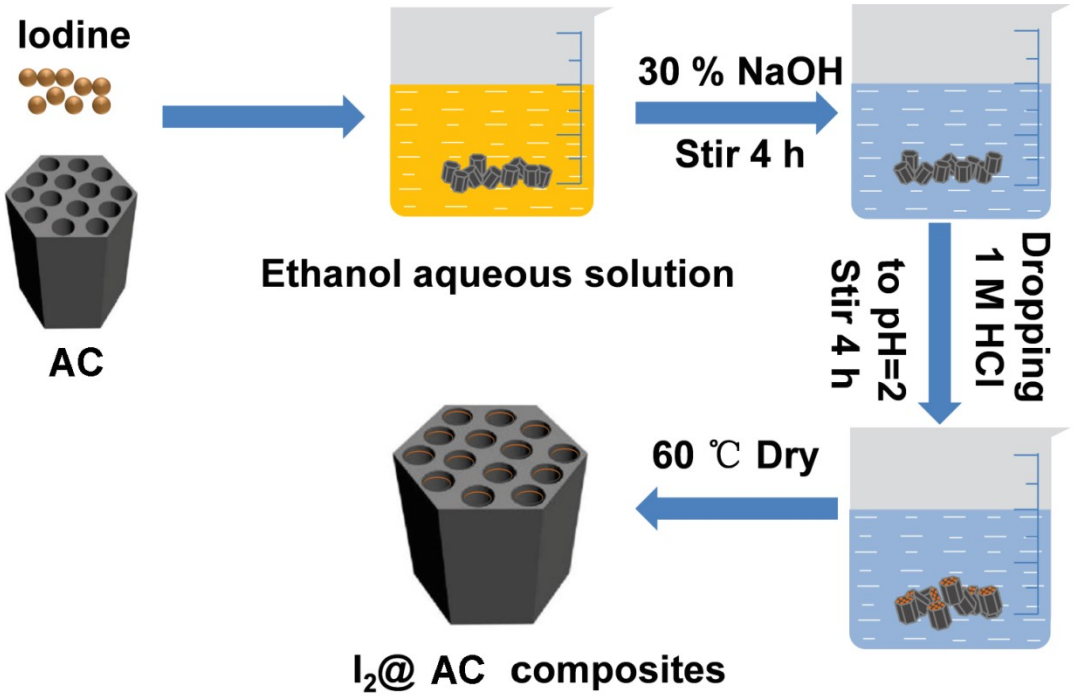

Figure S3. *In situ* deposition route of fabricating the I_2@AC composites.

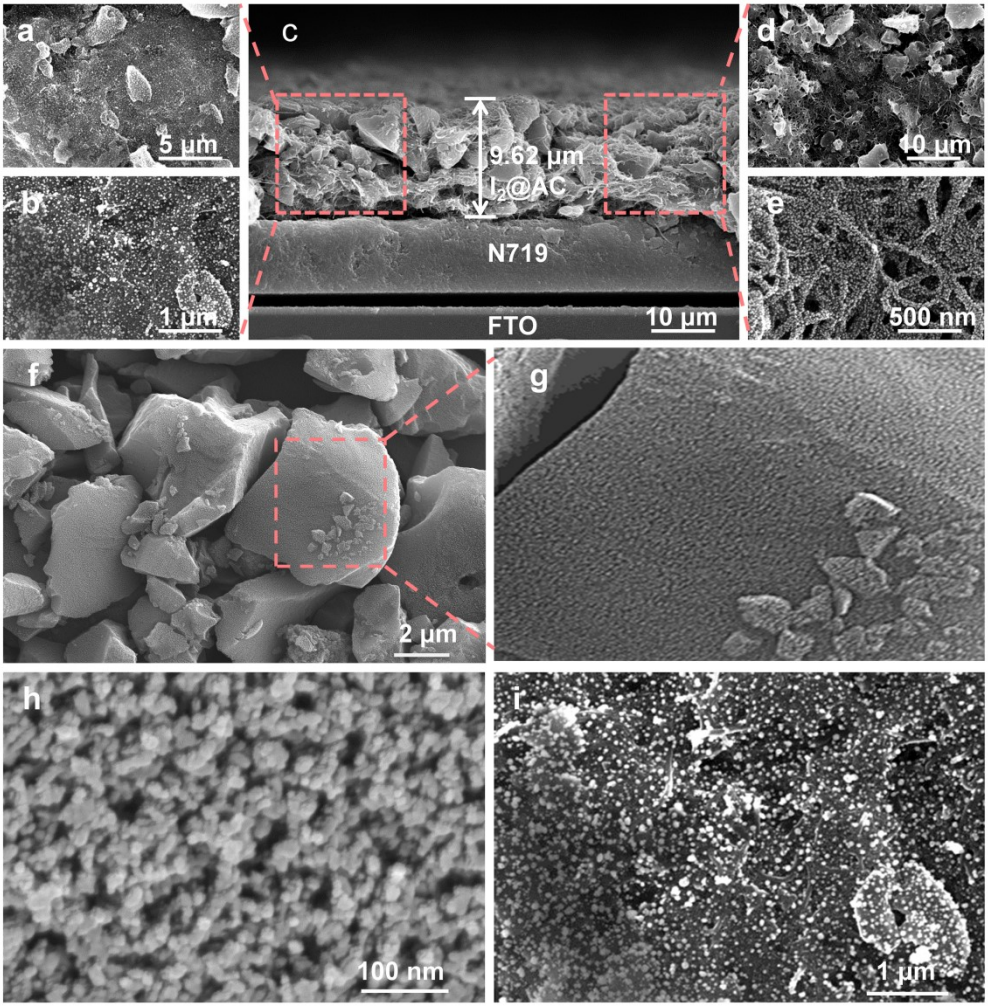

Figure S4. a) and b) SEM diagram of the battery charging to 2.8V. c) Cross-sectional view of the material coated on the FTO conductive glass. d) and e) SEM diagram of the battery discharging to 3.8V. f) Low and g) high-magnification SEM of the I_2@AC composites. Initial SEM diagram of the h) TiO_2 and i) the hybrid I_2@AC/N719-dye/TiO_2 photoelectrode.

Figure. S4a, S4b and **S4d, S4e** are SEM images of the photo-assisted rechargeable Li-I_2 battery after cyclic charging to 2.8V and 3.8V respectively. Element mapping in **Figure 2a-d** showed that the iodine ions generated by the reaction are uniformly attached to the surface of activated carbon. The I_2@AC composite is coated on the N719 sensitized upper layer, as shown in **Figure S4c**. **Figure S4f, S4g** are SEM images of the uncirculated I_2@AC composite material at low and high magnification, and the porous structure of activated carbon can be seen. The morphology of the mesoporous TiO_2 nanoparticle film is shown in **Figure S4h**, and the morphology of the integrated electrode of I_2@AC/N719-dye/TiO_2 is shown in

Figure S4i. It is observed that I_2@AC/N719-dye can be well adsorbed on the TiO_2 nanofilm surface, which can increase the efficiency of interfacial charge injection.

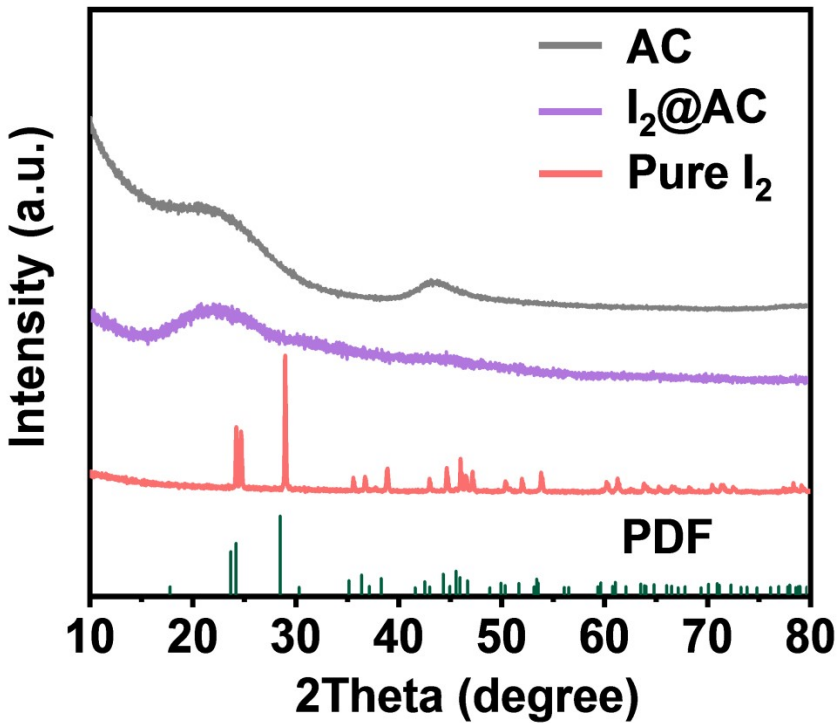

Figure S5. XRD patterns of pure iodine, pure AC and I_2@AC.

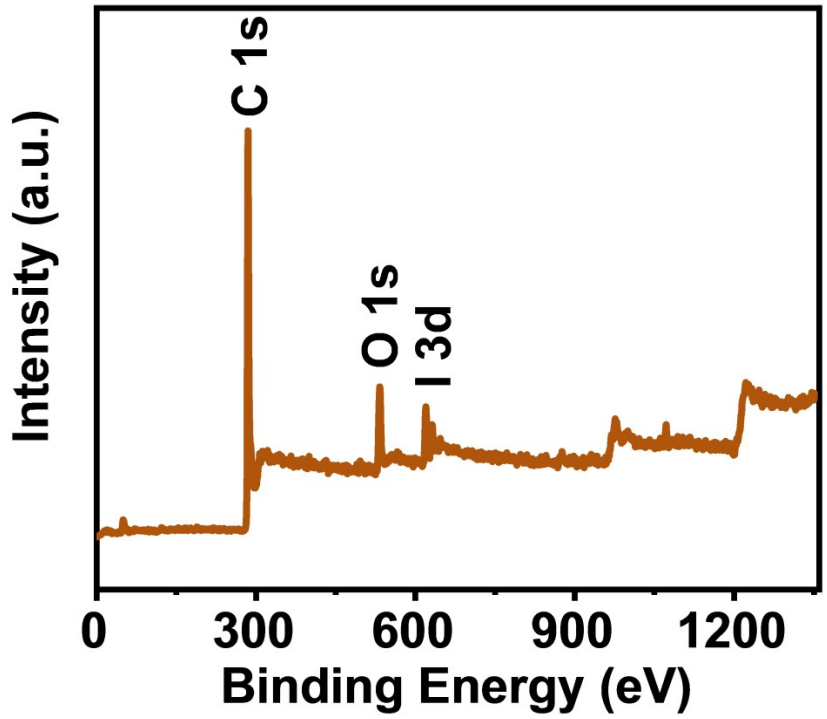

Figure S6. The XPS C 1s, I 3d, and O 1s peaks of I_2@AC composites.

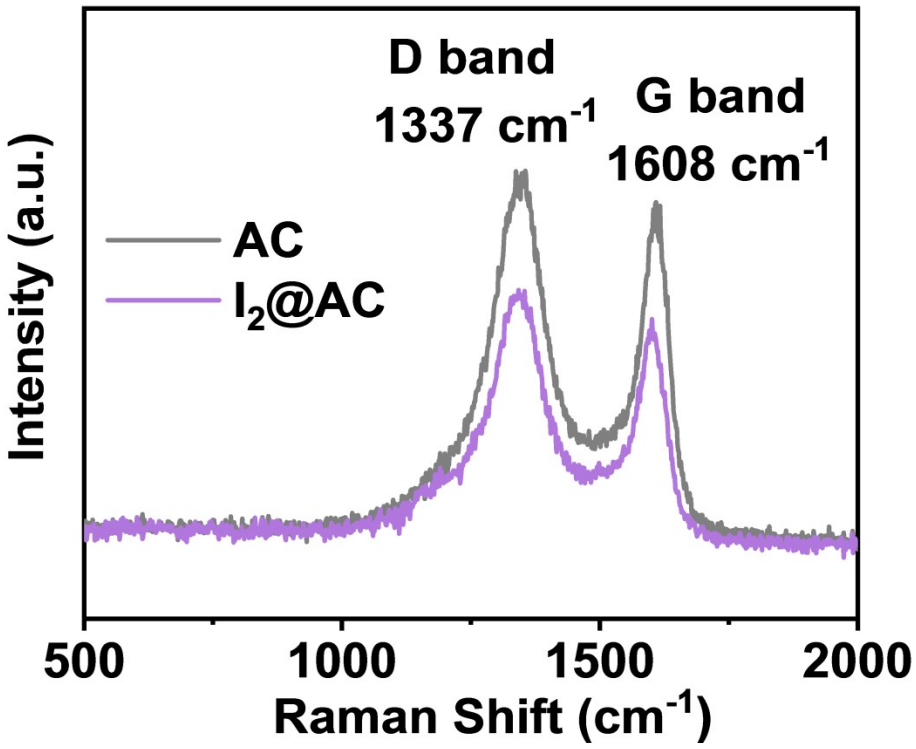

Figure S7. Raman spectra of pure iodine, pure AC and I_2@AC.

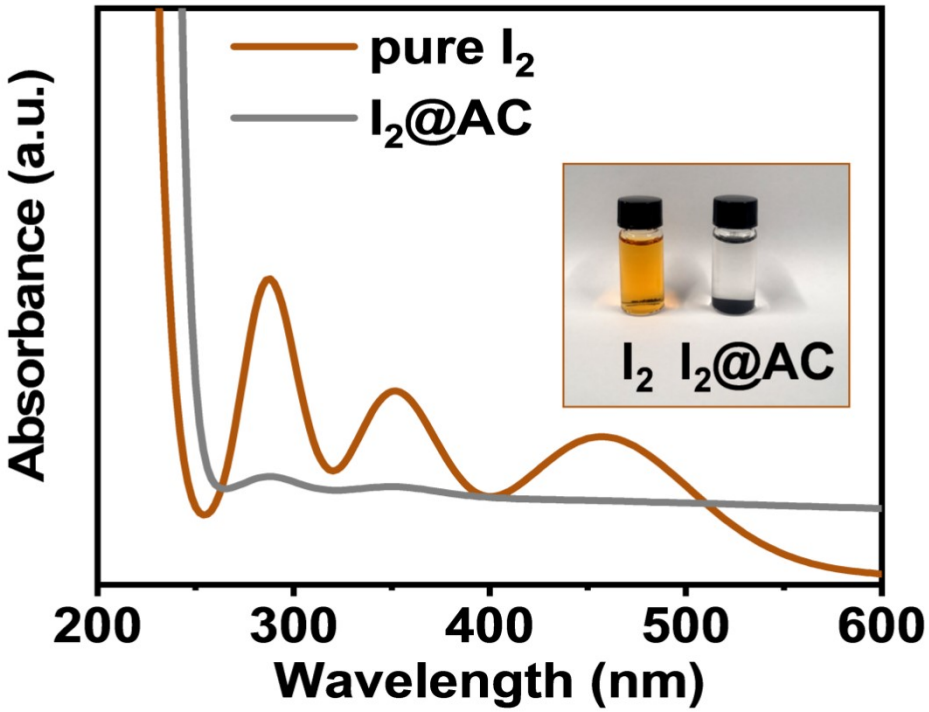

Figure S8. The UV-vis absorption spectra of I_2@AC composites and I_2.

Elemental iodine and I_2@AC composite materials were dissolved in ethanol aqueous solution. After one week, the solutions were tested by The UV-vis absorption spectra **(Figure S8).** The test results show that the I_2@AC composite material does not have an obvious peak of iodide ion, which verifies that iodine is very well adsorbed in the matrix AC.

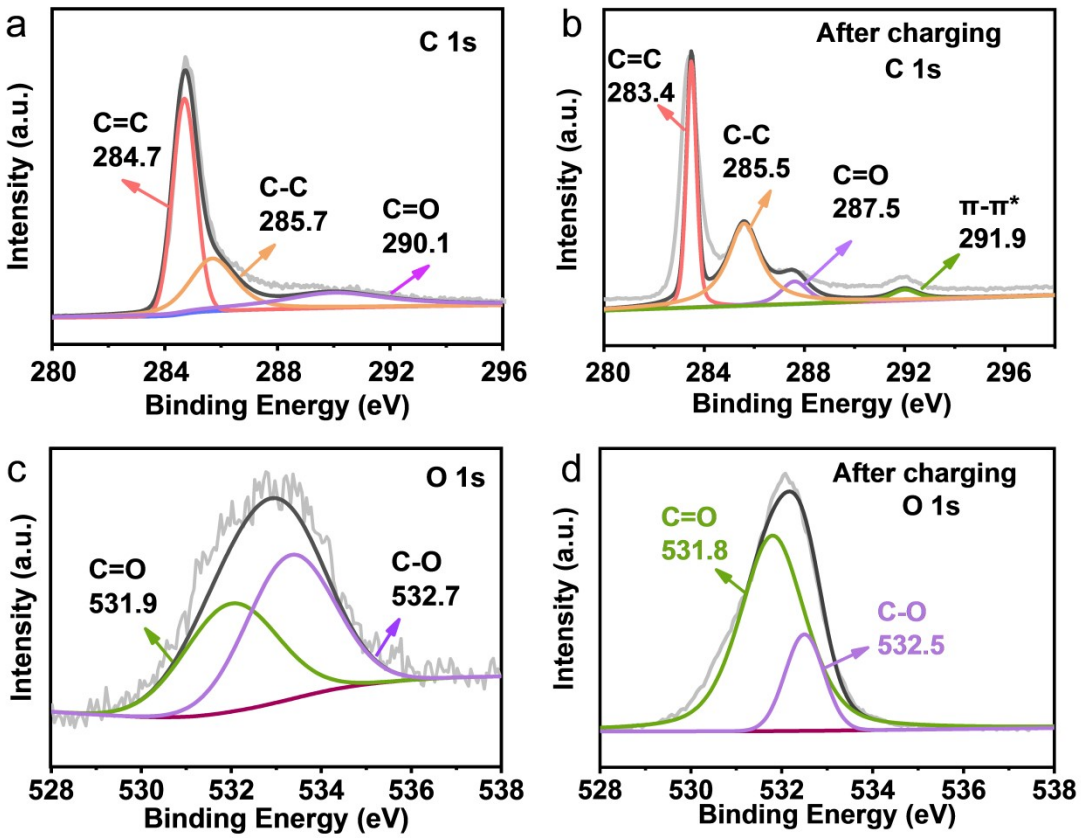

Figure S9. a and b) XPS peak of C1s before and after charging. c and d) XPS peak of O1s before and after charging.

As indicated in **Figure S9a**, the high-resolution C 1s spectrum shows that a main peak of 284.7 eV corresponds to C=C, and two sub-peaks are concentrated at 285.7 eV and 290.1 eV, corresponding to C-C and C=O.moreover, the high-resolution O 1s peak in **Figure S9c** corresponds to the C=O and C-O bond. After the illumination cycle, the intensity of C 1s peak increased, but the O 1s peak decreased significantly, as shown in **Figure S9b and S9d**, indicating the decrease of oxygen-containing functional groups.

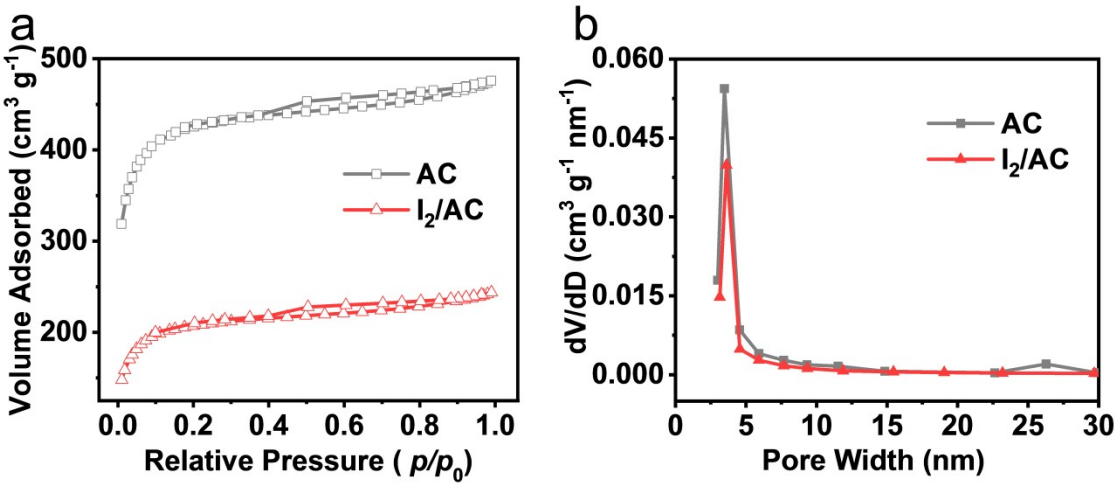

Figure S10. a)The inset shows the corresponding nitrogen sorption isotherms of AC and I_2@AC composites. b) The pore size distribution curve of AC and I_2@AC composites.

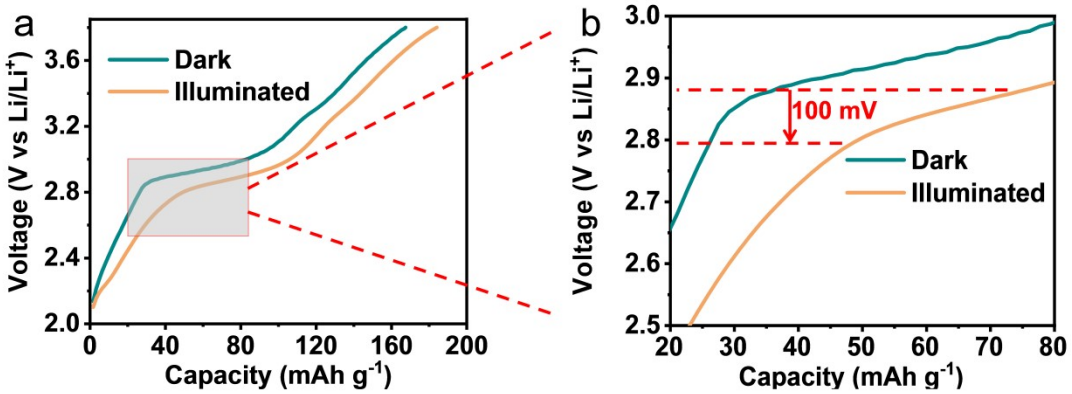

Figure S11. a) and b) The photoassisted charging curves at a current density of 100 mAh g^{-1} of the photoassisted chargeable Li-I_2 battery under the illumination.

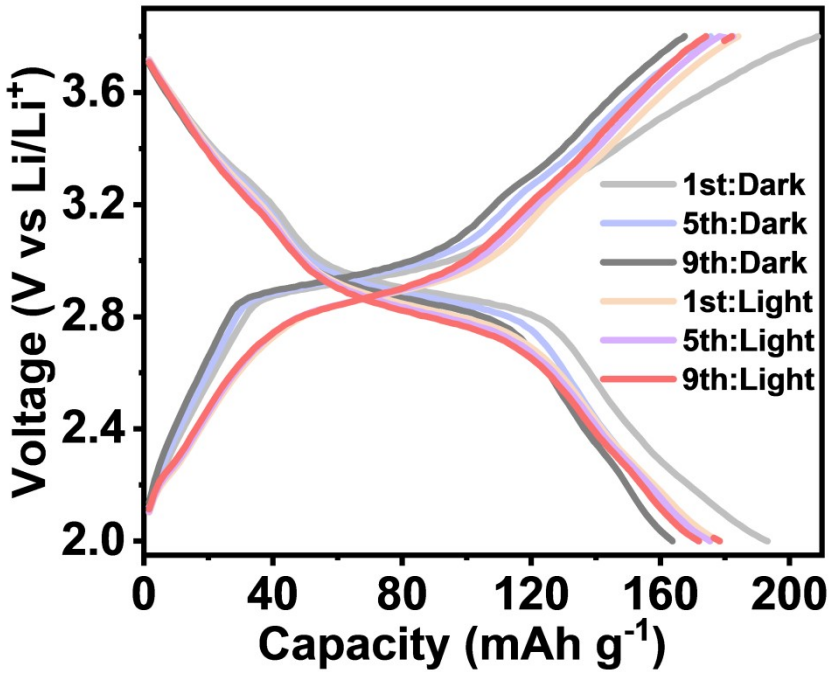

Figure S12. GCD curves at 100 mAh g^{-1} under dark and illuminated conditions.

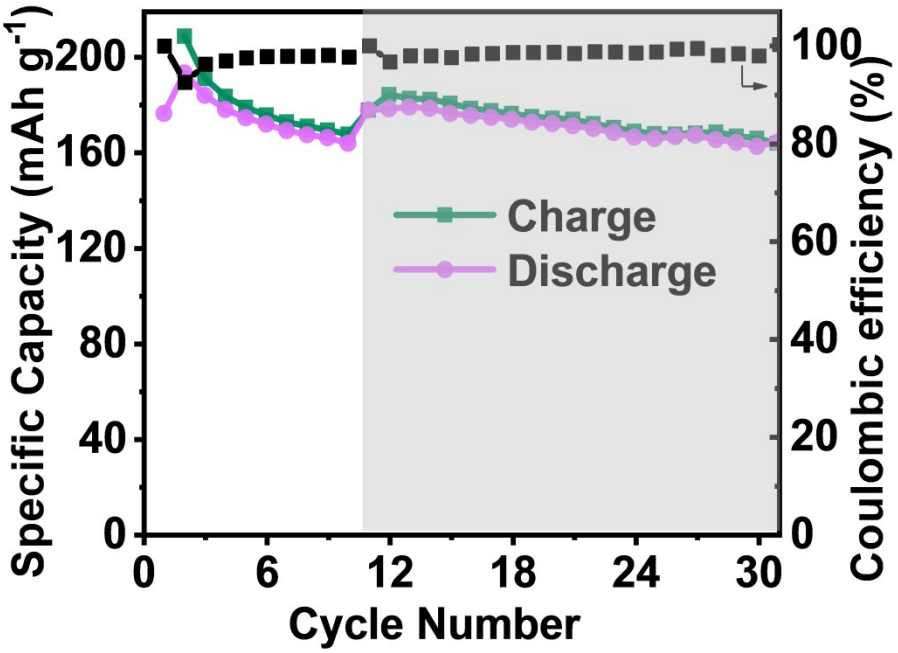

Figure S13. Cycle performance of the I_2@AC composites at 100 mAh g^{-1} rate under dark and illuminated conditions (the shaded region).

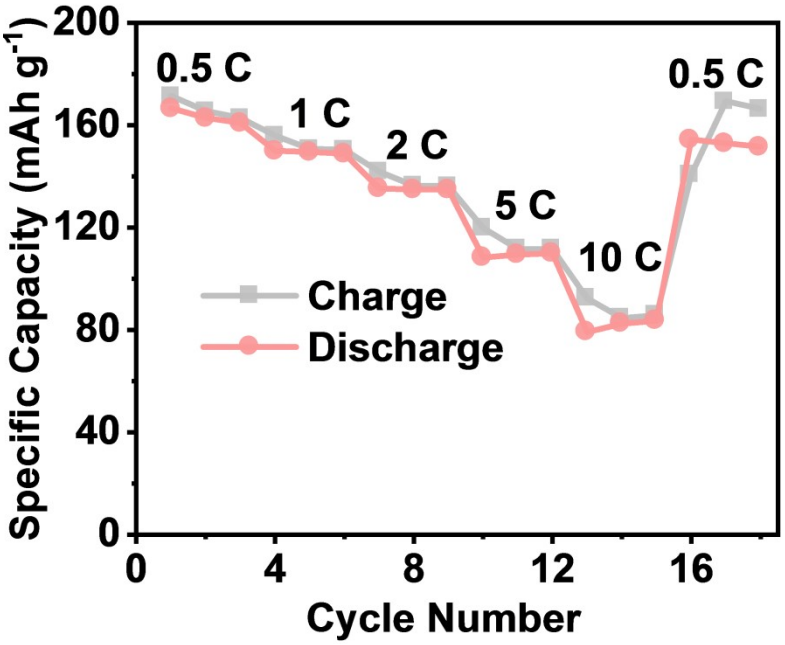

Figure S14. Rate capabilities of the as-prepared I_2@AC composites.

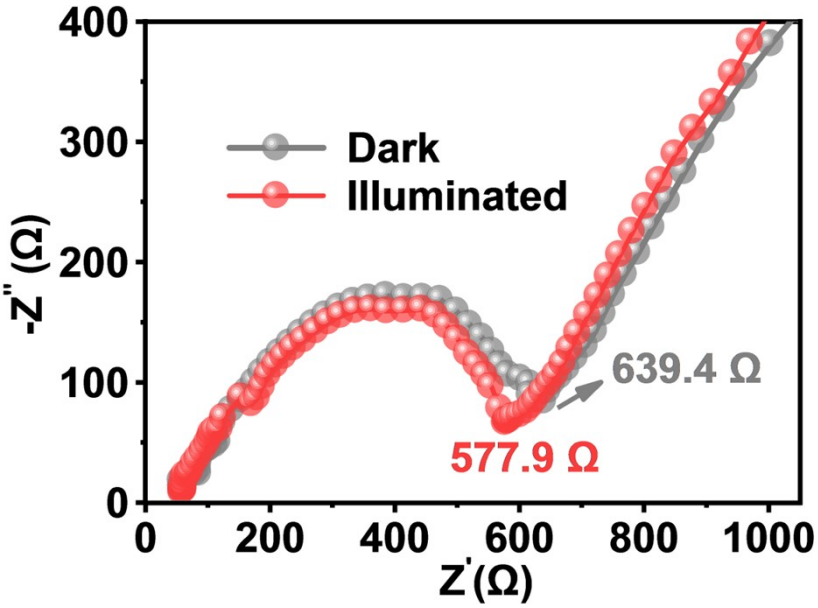

Figure S15. AC impedance spectra of the photoassisted rechargeable Li-I_2 battery in dark and illuminated conditions.

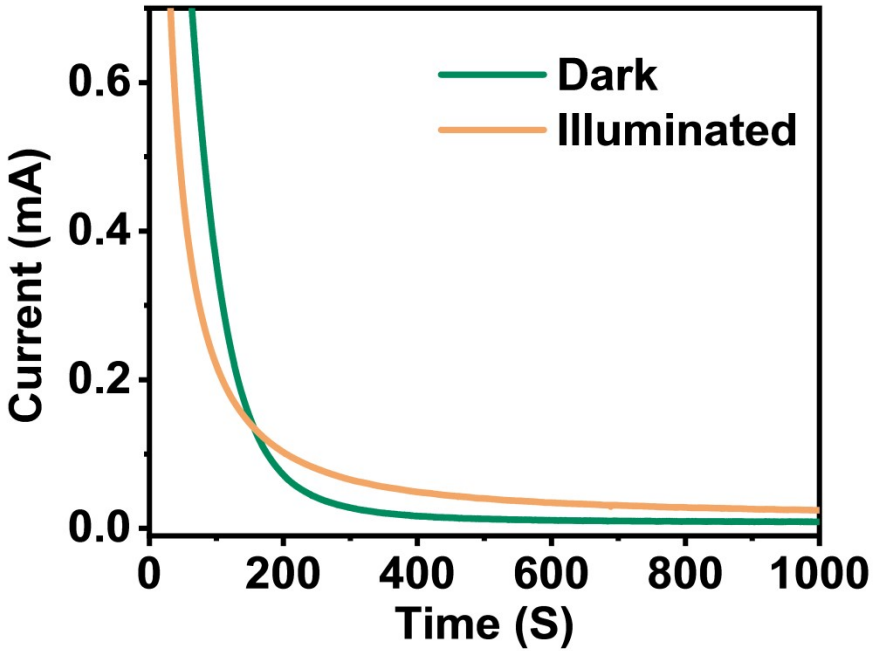

Figure S16. After fully discharged, the chronoampere curve of 1000 seconds of dark and illuminated under 3.1 V constant voltage charging.

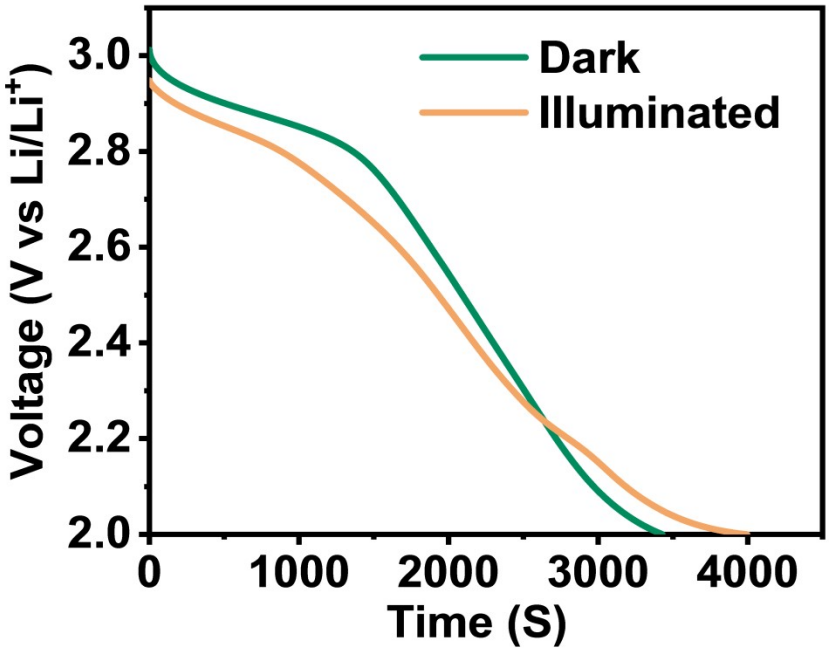

Figure S17. Constant current discharge curve after chronoampere test under dark and illuminated conditions.

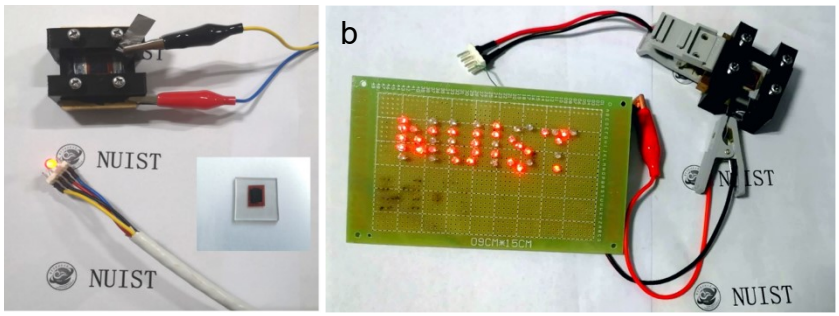

Figure S18. Optical photos of an LED bulb and grouped LED powered by a photo-assisted rechargeable Li-I_2 battery, the inset shows the prepared electrode sheet.

Table S1 A detail comparison of the performances of the recently reported Li-I_2 batteries. [2-7]

Battery Types	Photo electrode	photocharging voltage	Specific capacity	energy efficiency	Ref.
Aqueous Li-I_2 Battery	Dye z907	2.9 V	89 mAh g^{-1} (0.50 mA cm^{-2})	100 %	2
Aqueous Li-I_2 Battery	α-Fe_2O_3	3.43 V	160 mAh g^{-1} (0.50 mA cm^{-2})	95.4 %	3
chargeable Li-ion battery	TiO_2	2.78 V	137 mAh g^{-1} 0.04 mA cm^{-2}	121 %	4
Li-I_2 batteries (iodine/β-CD)	—	3.0 V	133mAh g^{-1} (105.5 mA g^{-1})	93 %	5
aqueous Zn-I_2 battery	TiO_2	0.56 V	83 mAh g^{-1} (0.5 mA g^{-1})	93 %	6
Aqueous Sodium-Ion Battery	TiO_2	0.08 V	110 mAh g^{-1} (0.50 mA cm^{-2})	111 %	7
Photo-assisted Li-I_2 Battery (This Work)	Dye N719	2.85 V	193 mAh g^{-1} (105.5 mA g^{-1})	93 %	**This Work**

The energy efficiency (η) of the photo-assisted battery can be expressed as:

$$\eta = E_{out} / E_{in} \times 100\ \%$$ [8]

Reference

1. M. Y. A. Rahman, A. A. Umar, R. Taslim and M. M. Salleh, *Electrochimica Acta*, 2013, **88**, 639-643.
2. M. Yu, W. D. McCulloch, D. R. Beauchamp, Z. Huang, X. Ren and Y. Wu, *Journal of the American Chemical Society*, 2015, **137**, 8332-8335.
3. Q. Zhang, Z. Wu, F. Liu, S. Liu, J. Liu, Y. Wang and T. Yan, *Journal of Materials Chemistry A*, 2017, **5**, 15235-15242.
4. Q. Li, N. Li, M. Ishida and H. Zhou, *Journal of Materials Chemistry A*, 2015, **3**, 20903-20907.
5. F.-s. Cai, Y.-q. Duan and Z.-h. Yuan, *Journal of Materials Science: Materials in Electronics*, 2018, **29**, 11540-11545.
6. Y. Man, Q. Hao, F. Chen, X. Chen, Y. Wang, T. Liu, F. Liu and N. Li, *ChemElectroChem*, 2019, **6**, 5872-5875.
7. Q. Li, N. Li, Y. Liu, Y. Wang and H. Zhou, *Advanced Energy Materials*, 2016, **6**, 1600632.
8. B. Deka Boruah, A. Mathieson, S. K. Park, X. Zhang, B. Wen, L. Tan, A. Boies and M. De Volder, *Advanced Energy Materials*, 2021, **11**, 2100115.